TU Delft

Delft University of Technology

Multi-objective optimal provision of fast frequency response from EV clusters

Sanchez Gorostiza, Francisco ; Gonzalez-Longatt, Francisco; Rueda, José Luis

DOI
10.1049/iet-gtd.2020.0717

Publication date
2020

Document Version
Accepted author manuscript

Published in
IET Generation, Transmission and Distribution

Citation (APA)
Sanchez Gorostiza, F., Gonzalez-Longatt, F., & Rueda, J. L. (2020). Multi-objective optimal provision of fast frequency response from EV clusters. *IET Generation, Transmission and Distribution*, *14*(23), 5580-5587. https://doi.org/10.1049/iet-gtd.2020.0717

Important note
To cite this publication, please use the final published version (if applicable).
Please check the document version above.

Copyright
Other than for strictly personal use, it is not permitted to download, forward or distribute the text or part of it, without the consent of the author(s) and/or copyright holder(s), unless the work is under an open content license such as Creative Commons.

Takedown policy
Please contact us and provide details if you believe this document breaches copyrights.
We will remove access to the work immediately and investigate your claim.

This work is downloaded from Delft University of Technology.
For technical reasons the number of authors shown on this cover page is limited to a maximum of 10.

This paper is a postprint of a paper submitted to and accepted for publication in
IET Generation, Transmission and Distribution and is subject to Institution of Engineering and Technology Copyright. The copy of record is available at the IET Digital Library.

Multi-Objective Optimal Provision of Fast Frequency Response from EV Clusters

Francisco Sánchez Gorostiza, *Student Member, IEEE*, Francisco Gonzalez-Longatt, *Member, IEEE*, and José L. Rueda, *Member, IEEE*

***Abstract*-- Declining levels of rotational inertia in modern power systems prompt transmission system operators (TSOs) to develop novel ways of maintaining the balance between generation and demand. Services such as fast frequency response (FFR) can help the TSO achieve this balance. The growing penetration of electric vehicles (EVs) promotes the provision of FFR from clusters of EVs. Fast charging stations are more geared towards destination charging, whereas slow charging stations are more attractive as providers of FFR, given the longer connection times. In this paper, the provision of FFR from EV clusters is formulated as a multi-objective optimisation problem with network security constraints and two minimisation objectives, i.e. the maximum frequency deviation following a disturbance and the energy provided by public EV charging stations. A methodology was developed to solve the optimisation problem with a variant of the nondominated sorting genetic algorithm (NSGA-II). This methodology allows the decision-maker to consider the trade-offs among the objectives, leading to a more informed decision. An enhanced frequency-responsive aggregate model (EFRAM) of a cluster of EVs was developed to study the provision of FFR in a multi-area power system. A three-area dynamic model of the Nordic power system was used to illustrate the performance of the proposed methodology.**

***Index Terms*—Aggregate models, electric vehicles, Pareto optimisation, system frequency response, vehicle-to-grid.**

I. Introduction

THE modern electricity system is securely managed by always matching the amount of power generation with the demand. However, several factors, including the massive integration of power-converter-based technologies, are affecting the total system rotational inertia [1]. Declining levels of rotational inertia have a negative effect on the system security and economic operation; especially following a significant power imbalance. Modern developments in the energy capacity and response time of battery energy storage systems (BESS), makes them an attractive alternative as providers of frequency control services of power systems with high penetration of non-synchronous generation [2]. One of these services is termed Fast Frequency Response (FFR) and refers to a rapid injection of active power to the grid in a timeframe of two seconds or fewer and proportional to the frequency deviation from its nominal value [2]. Beyond the classical BESS, the growing penetration of electric vehicles (EV) promotes an appealing option to provide ancillary services to the modern power system. The inherent charging flexibility of EVs, combined with smart charging functionalities, allow the user to provide highly valued ancillary services to the transmission system operator (TSO) [3], [4]. However, the energy stored in a single EV battery is not nearly enough to be of practical use to the TSO in grid-scale applications. Only when the combined action from a sufficiently large number of vehicles is aggregated, their effect can be useful and valuable to the TSO. Incidentally, the ongoing electrification of personal and commercial mobility worldwide enables and promotes these valuable ancillary services. Countries such as China and the USA already have a combined fleet of over 2 million EVs on their roads [5], while estimates from the Great Britain (GB) electricity system operator, NGESO, put the number of EVs on GB roads on up to 10 million by 2030 [6].

It has been generally accepted that the energy stored in the batteries of large groups of EVs can be tapped, via so-called Vehicle-to-Grid (V2G), to help the TSO in balancing tasks if the remaining capacity after the provision of the service is enough to cover the needs of the user [7]. Some analysts cast doubts on the commercial viability of the provision of V2G services from clusters of EVs, citing substantial connection costs and increased battery degradation as the most pressing concerns [8]. However, several think-tanks [9], energy companies [10] and EV manufacturers [11] worldwide, are presently running large-scale trials to explore the benefits of the service, and around half of those surveyed in a recent study showed a clear interest in delivering V2G services [12]. To provide adequate FFR services to the power system, sufficient EV charging infrastructure, either at public or private locations, needs to be in place and adequately distributed across the grid. Charging stations bigger than 22 kW, while able to replenish the average EV battery in minutes, take a considerable amount of the limited site capacity. Consequently, these rapid and ultra-rapid[1] chargers are better suited for destination charging at public locations such as supermarkets and forecourts and are

Manuscript received August 3, 2019; revised January XX, 2020;

Francisco Sánchez is with the Wolfson School of Mechanical, Electrical and Manufacturing Engineering, Loughborough University, Loughborough, UK (email: F.Sanchez@lboro.ac.uk).

Francisco Gonzalez-Longatt is with the Department of Electrical Engineering, Information Technology and Cybernetics, University of South-Eastern Norway, Porsgrunn, Norway (email: fglongatt@fglongatt.org).

José L. Rueda is with the Department of Electrical Sustainable Energy, Delft University of Technology, Delft, Netherlands (email: J.L.RuedaTorres@tudelft.nl).

[1] According to their speed, charging stations are classified into four groups: Slow (≤ 3 kW), Fast (7 – 22 kW), Rapid (43 – 120 kW) and Ultra-Rapid (> 120 kW) [5].

distributed across the transport network to encourage intercity journeys. Since the main point of rapid EV chargers is to replenish the state of charge (SoC) of the user's battery as quickly as possible, these units are not the best suited for the provision of FFR [13]. On the other hand, smaller chargers, such as the presently prevalent 7 kW, take a smaller portion of the available site capacity at the cost of increasing the average charging time to around 3 to 4 hours and are therefore more geared towards workplace or overnight private charging. Given their longer connection times, these units, become attractive for smart charging schemes and provision of ancillary services.

In this research paper, the question of how much energy to provide from each EV charging station, whilst delivering FFR services in a multiple area power system, is formulated as a multi-objective optimisation problem considering network security constraints. Two kinds of network security constraints are considered, i.e. those dealing with the rate of change of system variables and those related to the active power flow limitations between the different areas of the network. To represent more accurately the dynamic behaviour of the EV cluster while it delivers FFR services to the grid, this paper proposes an enhanced frequency-responsive aggregate model (EFRAM). The proposed EV model, centred on the work of [14], considers the distribution of the different parameters of the EVs inside the cluster as opposed to relying only on their average values.

To solve the optimisation problem, it is possible to set the frequency deviation as a constraint and get the EV cluster parameters that minimise its FFR energetic contribution. Alternatively, it is feasible to set an upper limit for the EV cluster injected energy and get the parameters that minimise the system frequency deviation. Instead, a multi-objective approach that allows visualising the trade-offs between the two objectives is followed in this paper. Specifically, the inertia-weighted maximum frequency deviation of the power system forms the first objective, whereas the total energetic contribution from the EV clusters is the second objective. The formulation as a multi-objective optimisation problem, with the frequency deviation acting as a goal instead of as a constraint, is helpful for two reasons. First, it dispenses with the need for choosing a penalty factor, as is traditionally required for handling constrained optimisation problems [15]. One drawback of the penalty function approach is the sensibility of the resulting solution to the chosen penalty factor [16]. A second advantage of the multi-objective formulation proposed in this paper is that it provides the decision-maker with more information about the interaction of the different objectives. Indeed, the output of the process is a family of optimal or close to optimal solutions instead of a single solution, which aids the trade-off analysis and supports the decision-making process.

A methodology is developed to solve the optimisation problem using an implementation of an elitist genetic algorithm variant of the *nondominated sorting genetic algorithm* (NSGA-II). This algorithm was chosen because of its efficiency in constraint handling coupled with its ability to outperform other genetic algorithms by finding solutions closer to the true Pareto-optimal front when a sufficient number of function evaluations is performed [17].

A. Literature Review

Most studies in system frequency response (SFR) optimisation have only focused on distributed energy resources (DERs) such as photovoltaic and wind energy systems, and in most cases, dealing only with the optimisation of a single function, typically system losses or frequency deviation [18], [19]. In [18], the optimal droop parameters of the DERs on a distribution network were derived analytically to allocate the active power injected equitably among the DERs. The location and size of a BESS to minimise load shedding in a transmission system was studied in [19] though it was formulated as a single-objective optimisation problem, i.e. the location was selected *a priori*, based on system-specific considerations and then, the size of the BESS was obtained by solving a constrained optimisation problem with an adaptation of a genetic algorithm. In [20], the total energy cost and network losses from the charging of single-phase EVs were combined for minimisation into an augmented objective function. Fuzzy membership functions were employed to derive the weights assigned to each part of the augmented objective function. A limitation of this approach is that, since both objective functions are combined, it is not possible to directly visualise the Pareto-optimal front.

B. Paper Contributions

The main contributions of this paper are: (i) Developing a frequency-responsive model of a cluster of EVs providing FFR that yields adequate results for different measurement delays and which can be included in multi-area power system studies (see Section II), (ii) Developing a methodology, using NSGA-II, to find the Pareto-optimal fronts when minimising the system frequency deviation and EV cluster injected energy following a load disturbance under different power system scenarios (see Section III.A), and (iii) Including realistic TSO imposed network security constraints in the problem formulation related to the rate of change of frequency and injected power as well as with inter-area power flows (see Section III.D).

II. System Frequency Response

This section describes the dynamic model used to represent the aggregated response of a cluster of EVs providing FFR services. Next, a multi-area representation of the power system, including EV clusters, is developed for the study of the SFR.

A. Enhanced Frequency-responsive Aggregate Model (EFRAM)

This paper proposes an *enhanced frequency-responsive aggregate model* (EFRAM) to represent a cluster of EVs providing FFR. The proposed EFRAM leverages the existing research in aggregate modelling of EV clusters [14], [21] and combines it with a frequency-responsive control for the provision of FFR, as shown in Fig. 1. A first-order transfer function is used to represent the EV charger dynamic with the time constant (T_{EV}). The EFRAM uses the Laplace transformation of the cumulative distribution function (CDF) of the time delay as suggested in [14] to reduce the error that

appears when the time delay of the EVs in the cluster is widely distributed.

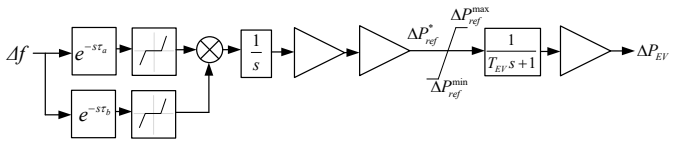

Fig. 1. Enhanced frequency-responsive aggregate model (EFRAM) for the provision of FFR from a cluster of EVs.

The EFRAM considers that the change in the output power from the EV cluster (ΔP_{EV}), as a consequence of a frequency deviation, can be described by the following equation:

$$\Delta P_{EV}(s) = \frac{k_{cluster} k_{droop} k_{agg}}{s\left(T_{EV} s + 1\right)} \left(e^{-s\tau_a} - e^{-s\tau_b}\right) \Delta f(s) \qquad (1)$$

where k_{droop} is the aggregate droop constant of the EV cluster which relates the locally measured frequency deviation with the reference power output [22], and k_{agg} is the delay distribution constant which value depends on the boundaries of the time delay distribution, as described by:

$$k_{agg} = \frac{1}{\tau_b - \tau_a}, \quad \tau_b > \tau_a \qquad (2)$$

The parameters τ_a and τ_b make up the bounds of the delay distribution, and their value depends on the probability distribution function (PDF) of the EV cluster measurement time delay. Table I shows two useful approximations of the aggregation bounds for the case when the time delay follows a uniform (U) or a normal (N) distribution [14].

TABLE I
AGGREGATION BOUNDS FOR THE TIME DELAY IN THE EV CLUSTER.

Time delay PDF	*Lower bound τ_a*	*Upper bound τ_b*
$U[t_L,t_U]$	t_L	t_U
$N[\mu,\sigma]$	μ - 2σ	μ + 2σ

The effects from the number of V2G enabled EVs in the cluster, the rated power of the charging stations and the power base of the system for per unit calculations, are summarised in the EV cluster constant ($k_{cluster}$), defined as follows:

$$k_{cluster} = \frac{\alpha N_{EV} P_{cluster}}{P_{base}} \qquad (3)$$

where α represents the fraction of EVs that can provide V2G services for FFR, N_{EV} is the number of EVs in the cluster, $P_{cluster}$ is the rated power of the charging stations, and P_{base} is the power base of the system for per unit calculations.

The EFRAM includes a dead band in the provision of FFR to avoid unnecessary charging/discharging events for small frequency deviations. This implies that for values of frequency deviation with a magnitude smaller than the dead band, there is no FFR from the EV cluster. The normalised reference output from the EV frequency controller (ΔP^*_{ref}) is bounded in the range [$\Delta P^{\min}_{ref}$, $\Delta P^{\max}_{ref}$] by a limiter block.

B. Multi-area Model Including EFRAM

In this section, an equivalent frequency response model for a multi-area power system is modified to include the EFRAM. The starting point is the classic SFR model of a single isolated power system, which is extended to form an interconnected network comprising N control areas connected by tie-lines. Fig. 2 shows the SFR model of the i-th control area. It contains several EV clusters that represent charging stations with different characteristics.

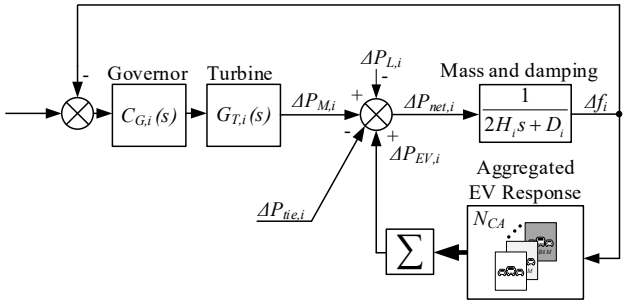

Fig. 2. Block diagram depicting the i-th control area in a multi-area SFR model considering the EFRAM aggregated FFR from clusters of EVs.

The aggregated response from the EV clusters connected in the i-th area is denoted $\Delta P_{EV,i}$. The frequency deviation (Δf_i) following a load disturbance ($\Delta P_{L,i}$) in the i-th control area can be described by the following equations in the Laplace domain:

$$\Delta P_{M,i}(s) - \Delta P_{L,i}(s) + \Delta P_{EV,i}(s) - \Delta P_{tie,i}(s) = \Delta P_{net,i}(s) \qquad (4)$$

$$\Delta f_i(s) = \frac{\Delta P_{net,i}(s)}{2H_i s + D_i} \qquad (5)$$

where $\Delta P_{M,i}(s)$ is the increment in the mechanical power and the term $\Delta P_{EV,i}(s)$ corresponds to the change in the injected power from the i-th EV cluster to the grid following a frequency deviation. Transfer functions $C_{G,i}(s)$ and $G_{T,i}(s)$, model the effect that different types of turbine and generator (e.g. thermal, hydro) have on the SFR. The equivalent model lumps the effects of the system loads and generators into a first-order transfer function that considers equivalent inertia constant (H_i) and a single damping constant (D_i) for each control area.

High voltage transmission lines or tie-lines interconnect the different areas of the multi-control-area power system considered. The net tie-line power interchange of each area ($\Delta P_{tie,i}$) can be expressed in vector notation ($\mathbf{\Delta P_{tie}}$) as:

$$\mathbf{\Delta P_{tie}} = \frac{2\pi}{s} \mathbf{L} \cdot \mathbf{\Delta f} \qquad (6)$$

$$\Delta P_{tie,i} = \sum_{\substack{j=1 \\ j \neq i}}^{N} \Delta P_{i,j} \quad \forall i = 1, \ldots, N \qquad (7)$$

where $\mathbf{\Delta P_{tie}} = [\Delta P_{tie,1}, \ldots, \Delta P_{tie,N}]^{\mathrm{T}}$ is a vector in which the i-th component is equal to the net tie-line power exchange of the i-th area ($\Delta P_{tie,i} > 0$ implies that the i-th area is a net exporter); $\Delta P_{i,j}$ represents the change in the power flow on the transmission line between control areas i and j; $\mathbf{\Delta f} = [\Delta f_1, \ldots, \Delta f_N]^{\mathrm{T}}$ is a vector that contains the frequency deviation for each control area following a load disturbance or an inter-area power flow fluctuation; $\mathbf{L}$ corresponds to the Laplacian matrix of the underlying network graph, weighted by the synchronising torque coefficients ($T_{i,j}$) and with their elements defined as follows:

$$L_{i,i} = \sum_{\substack{j=1 \\ j \neq i}}^{N} T_{i,j} \text{ and } L_{i,j} = -T_{i,j} \qquad (8)$$

A power mismatch vector, given by $\mathbf{\Delta P_L} = [\Delta P_{L,1}, \ldots, \Delta P_{L,N}]^{\mathrm{T}}$

is defined, with its i-th component, $\Delta P_{L,i}$, indicating the power imbalance in the i-th area following a disturbance. The system inertia vector, defined as $\mathbf{H} = [H_1,\ldots,H_N]$, is formed by the inertia constant of each area's equivalent synchronous generator (on a common power base) and the scalar quantity ρ is defined as the inverse of the sum of all the elements of $\mathbf{H}$ as follows:

$$\rho = \left[\sum_{i=1}^{N} H_i\right]^{-1} \tag{9}$$

From the above definitions, it is straightforward to get the frequency deviation of the centre of inertia, Δf_{COI} as follows:

$$\Delta f_{COI}(s) = \rho\left(\mathbf{H}\Delta\mathbf{f}\right) \tag{10}$$

In this research paper, the frequency deviation from each area is scaled by its inertia constant; therefore, entailing a minimisation of the frequency deviation of the inertial centre. This variable is of interest for highly meshed grids, as it represents the aggregation of each area's frequency into the frequency of a single representative area.

III. Multi-objective Formulation

In this section, the provision of FFR from clusters of grid-connected EVs is formulated as a multi-objective optimisation problem with TSO imposed constraints. The parameters of the EV clusters are adjusted to fulfil the minimisation of two objectives: (i) the inertia-weighted maximum frequency deviation, and (ii) the energy contribution from the EV clusters following a loss of generation in the power system.

A. Mathematical Formulation

The multi-objective optimisation problem is that of simultaneously minimising the m objectives $F_i(\mathbf{x})$, $i = 1,\ldots,m$, of a control variable vector $\mathbf{x} = [x_1,\ldots,x_n]$, with n elements. The objective function is formulated as a vector of the different objectives $\mathbf{F(x)} = [F_1(\mathbf{x}),\ldots, F_m(\mathbf{x})]$ and can be described as:

$$\begin{aligned} &\min\ \{\,\mathbf{F}(\mathbf{x})\,\} \\ \text{Subject to:}\quad &\mathbf{G}(\mathbf{x}) = [g_j(\mathbf{x})] = 0 \quad \forall j = 1,\ldots, n_{eq} \\ &\mathbf{H}(\mathbf{x}) = [h_l(\mathbf{x})] \le 0 \quad \forall l = 1,\ldots, n_{ineq} \\ &x_k^l \le x_k \le x_k^u \ \ \forall k = 1,\ldots,n \end{aligned} \tag{11}$$

where n_{eq} corresponds to the number of equality constraints and n_{ineq} is the number of inequality constraints. The set of equality constraints is grouped into a vector denoted $\mathbf{G}(\mathbf{x})$. The vector of inequality constraints is designated $\mathbf{H}(\mathbf{x})$ and contains n_{ineq} inequality constraints. The function $g_j(\mathbf{x})$ corresponds to the j-th equality constraint, whereas $h_l(\mathbf{x})$ corresponds to the l-th inequality constraint. The k-th control variable is bounded inside the range $[\,x_k^l\,,\,x_k^u\,]$.

If any element of the objective function vector $\mathbf{F(x)}$ is competing with another, there is no unique solution to the optimisation problem. Any solution in which an improvement in one objective also carries a detriment in another function is denoted as a *non-inferior solution*. The goal of the multi-objective optimisation is, therefore, to obtain the non-inferior solutions of the objective function, also known as the *Pareto-optimal front*.

B. Control Variables

In this paper, the control variable vector is formed by the frequency droop coefficients of the EV clusters, denoted as:

$$\mathbf{x} = \left[k_{droop,i,j}\right] \ \ \forall i = 1,\ldots N\ ,\ \forall j = 1,\ldots N_{CA} \tag{12}$$

where $k_{droop,i,j}$ is the droop coefficient of the j-th EV cluster inside control area i and N_{CA} is the number of EV clusters in each control area.

C. Objective Functions

Two objective functions are considered in this paper. The first objective function (F_1) corresponds to the minimisation of the overall maximum frequency deviation following a disturbance in the j-th control area, expressed as:

$$F_1(\mathbf{x}) = \sum_{i=1}^{N} k_i\left(f_N - f_{\min,i}\right) = \sum_{i=1}^{N} k_i \Delta f_{\max,i} \tag{13}$$

where f_N is the rated frequency of the system, $f_{min,i}$ is the minimum frequency of the i-th control area following a step load disturbance (see Fig. 3). The difference between the system's nominal frequency and the minimum frequency obtained in control area i, is defined as $\Delta f_{\max,i}$. The term k_i represents a weighting factor in prioritising the system frequency response in the i-th area and N is the number of control areas in the power system model. In this paper, the weighting factors for each area are selected proportionally, according to the area's inertia constant i.e. $k_i = \rho H_i$.

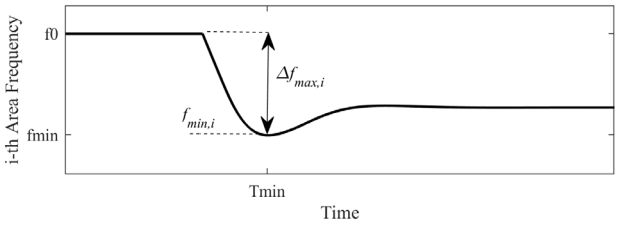

Fig. 3. Frequency response in the i-th area following a loss of generation.

The second objective function (F_2) corresponds to the minimisation of the total energy contributed to FFR by specific clusters of bidirectional EVs following a disturbance in area k, expressed as:

$$F_2(\mathbf{x}) = \sum_{i=1}^{N} W_{i,j_0}^{EV} = \sum_{i=1}^{N}\left(\int_0^{T_0} \Delta P_{i,j_0}^{EV}(t)dt\right) \tag{14}$$

where $W^{EV}{}_{i,j0}$ represents the energetic contribution to the FFR scheme from the cluster of vehicles j_0 providing V2G services in control area i, within a specified time frame T_0. The change in power consumption from EV cluster j_0 in the i-th control area is denoted $\Delta P^{EV}{}_{i,j0}$. $\Delta P^{EV}{}_{i,j0} > 0$ implies a reduction in the power consumption of the EV cluster or, an increase in the net power injected from the cluster in V2G modality. $\Delta P^{EV}{}_{i,j0} < 0$ implies an increase in the power consumption of the cluster or, a reduction of the power injected in a V2G scheme.

A higher droop value has the effect of reducing the maximum frequency deviation [2]. However, (1) implies that the energy contribution from the EV cluster following a disturbance depends on the selected droop value, and consequently, the selected objective functions are conflicting so a trade-off must be performed (see Fig. 4).

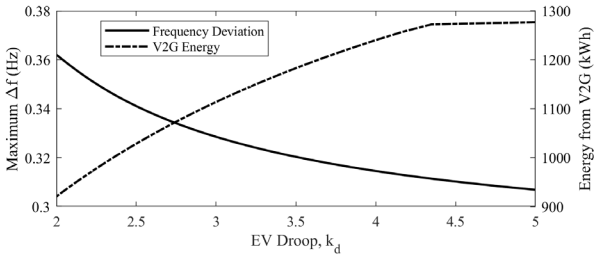

Fig. 4. Maximum frequency deviation and energy injected from V2G clusters for different values of the EV droop constant.

D. Constraints

The minimisation problem formulated in (13) and (14) includes two network security inequality constraints imposed by the TSO. These constraints are divided into two major groups. The first group includes constraints related to the rate of change of system variables and includes limitations for the rate of change of injected power from EV clusters and for the rate of change of the system frequency in each control area. The second group of constraints includes inter-area power flow limitations.

1) Rate of Change Constraints

A nonlinear inequality constraint related to a limitation in the rate of change of the injected power from the EV cluster is included in the formulation. This constraint can be stated as:

$$h_1(\mathbf{x}) = \frac{d\Delta P_{i,j}^{EV}}{dt} - \kappa_{ij} \le 0\,, \quad \forall i = 1,...,N \quad \forall j = 1,...,N_{CA} \tag{15}$$

where $\kappa_{i,j}$ represents the TSO imposed limit to the discharging rate of the EV cluster j in the i-th control area.

The rate of change of frequency (ROCOF) is limited by the TSO to avoid the spurious triggering of anti-islanding protection devices [24]. This constraint is expressed as:

$$h_2(\mathbf{x}) = \left|\frac{d\Delta f_i}{dt}\right| - ROCOF_i^{\max} \le 0 \quad \forall i = 1,...,N \tag{16}$$

where $|d\Delta f_i/dt|$ is the absolute value of the maximum frequency rate of change in the control area i, which is limited to be less than or equal to $ROCOF_i^{\max}$.

2) Inter-area Power Flow Constraints

To avoid overloading of inter-area transmission lines and the associated risk of cascade failure, the power flows between the control areas are constrained below a maximum value. The inter-area power flow constraint can be written as:

$$h_3(\mathbf{x}) = \left|P_{i,j}\right| - P_{i,j}^{\max} \le 0 \;\; \forall i = 1,...,N \;\; \forall j = 1,...,N_{CA}\,, \quad \forall i < j \tag{17}$$

where $|P_{i,j}|$ corresponds to the absolute value of the power flow between control area i and control area j and $P^{max}_{i,j}$ represents the maximum acceptable value of power flow between control area i and control area j given by the TSO.

E. Nondominated Sorting Genetic Algorithm II (NSGA-II)

In this paper, NSGA-II is used to find the Pareto-optimal front of multiple objective functions. NSGA-II has been used extensively in the literature as it is one of the most computationally efficient multi-objective optimisation algorithms available [25], [26]. Among the advantages of using an evolutionary algorithm to perform a multi-objective optimisation is that these kinds of algorithms naturally handle multiple solutions per iteration, and each iteration produces multiple trade-off solutions.

The nonlinear constraints are included via the simple and widely used *Penalty Function* algorithm [27]. The constrained optimisation problem is turned into an unconstrained one by the addition of a penalty term to the objective function. Unfeasible solutions, therefore, have their fitness value changed as they do not abode with the imposed constraints. After this modification, an unconstrained optimisation algorithm can be applied to solve the problem efficiently. Penalty factors are updated considering the hybrid optimisation scheme described in [28] to prevent scaling issues among the different constraints which might potentially skew the operation of the algorithm. An initial population of size P_0 is randomly generated by the algorithm. The fitness of each individual in the population is evaluated, and new individuals are created by the combination (tournament selection and mutation) of current individuals. Some individuals are removed from the population to make room for the evolved individuals. These new individuals are inserted into the population, and their fitness is evaluated, making a new generation. The maximum number of function evaluations is given by:

$$N_{feval} = P_0\left(1 + N_{gen}\right) \tag{18}$$

where N_{gen} is the maximum number of generations and P_0 is the initial population. The additional generation stems from requiring the evaluation of the initial population prior to the evolution of further individuals.

Key performance indicators such as the average Pareto spread and average Pareto distance are computed after each generation. The optimisation ends when the maximum number of generations is attained. This process, based on aspects of natural evolution, gives rise to a population of individuals that are better suited to their environments, as measured by their fitness function, than their ancestors.

IV. Illustrative Example

To illustrate the proposed multi-objective optimisation methodology, a three-area model of the Nordic power system, including clusters of EVs providing FFR, is considered and the Pareto-optimal fronts for different network scenarios are obtained. The power system model comprises three control areas representing the interconnected electrical networks of Sweden, Norway and Finland. A second-order low-pass filter (T_f = 0.5 s) is connected to the net inter-area power exchange block to smooth out the high-frequency components present in the model [29]. The power system models and optimisation routines are developed in MATLAB® R2018b.

In this illustrative case, the interest lies in minimising the energy injected from the public charging EVs while diminishing the maximum frequency deviation that follows a disturbance. Since the relative weights of the two objective functions depend on different external factors such as market and regulation in the area, they cannot be determined a priori.

Thus, a wide Pareto-front with several representative solutions is required.

A. EV Penetration Nordic System and Model Parameters

The Nordic block of countries makes up the third-largest EV market by volume of sales worldwide behind China and the United States [30]. At the end of 2018, the number of EVs in Norway stands out at over 249,000 units. This makes up over 70% of the EV stock in the Nordic countries and more than double the fleet of Sweden, the second-largest EV market in the region with over 78,000 EVs in circulation. The EV stock of Finland is around 12,000 vehicles at the end of 2018.

Norway leads the Nordic block in terms of publicly accessible EV chargers (fast and slow) at over 12,000, while Sweden and Finland trail behind with 7,000 and 931 chargers, respectively. However, less than 6% of the EV charging outlets in the region are installed in public areas, highlighting the importance of private charging (either at home or work) [30]. The combined number of EV chargers in the region (public and private) almost reached 264,000 at the end of 2017 [30]. In this region, FFR from V2G enabled charging stations and fast active power injection from hydro plants, compete for the frequency regulation market [31]. The fraction of vehicles able to offer FFR via V2G is estimated at 5% for private charging EVs and 1% for publicly charging EVs [32]. Authors in [33] indicated that the typical range for the time delay is between 150 ms and 2.0 s, while typical values for T_{EV} lie between 35 to 100 ms [34]. An average first-order time delay of 35 ms for the private chargers and 50 ms for the public chargers is considered [34].

The index i is used for enumerating the areas as follows: Sweden, Norway and Finland, so the characteristics of the EV clusters considered in the study are N_{ev1} = 78,630, $N_{ev,2}$ = 249,000, $N_{ev,3}$ = 12,050. $P_{2,1}^{\max}$ = 4.15 GW [29], $P_{3,1}^{\max}$ = 2.7 GW [29], $P_{2,1}^{N}$(@ 19:00 h) = 1.59 GW, $P_{3,1}^{N}$(@ 19:00 h) = -2.1 GW, $\kappa_{1,1} = \kappa_{2,1} = \kappa_{3,1}$= 40 MW/s, $\kappa_{1,2} = \kappa_{2,2} = \kappa_{3,2}$ = 40 MW/s, $\alpha_{1,1} = \alpha_{2,1} = \alpha_{3,1}$ = 5%, $\alpha_{1,2} = \alpha_{2,2} = \alpha_{3,2}$ = 1%, $T_{EV,1,1} = T_{EV,2,1} = T_{EV,3,1}$ = 35 ms, $T_{EV,1,1} = T_{EV,2,2} = T_{EV,3,2}$ = 50 ms, $ROCOF^{\max}_1 = ROCOF^{\max}_2 = ROCOF^{\max}_3$ = 0.5Hz/s.

B. Optimisation Algorithm Parameters

To arrive close to the Pareto-optimal front using NSGA-II, it is necessary to perform many function evaluations, usually costly in terms of computation time [35]. The number of function evaluations increases with both the population size and the number of generations. In this paper, the population size is established at 200, as it represents a compromise between the computational resources used and the level of detail in the solutions obtained [36]. To determine the minimum number of generations that would produce an accurate Pareto-front, the minimum of the sum of the equally weighted objective functions given by (13) and (14) is tracked alongside the number of generations. Fig. 5 shows the sum of the equally weighted objective functions, plotted against the number of generations, for 30 independent runs of the optimisation procedure, and in which each colour represents a different run. Irrespective of the randomness involved in the NSGA-II algorithm, it converges to a steady value after around 40 generations with the population size selected. Consequently, the maximum number of generations is selected as N_{gen} = 40.

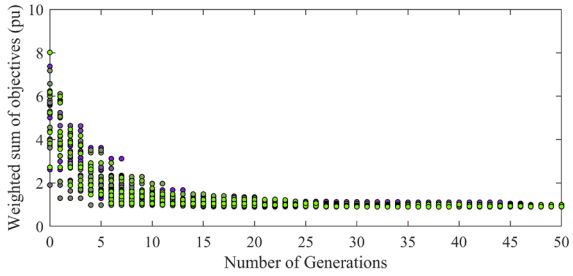

Fig. 5. The best-weighted sum of objectives vs the number of generations.

The crossover and Pareto fractions are set to 0.8 and 0.35 respectively, whereas the migration fraction is fixed to 0.2 and the migration interval is adjusted to 20. An initial penalty factor of 10 is selected [28] while the stopping criteria comprise reaching the maximum number of generations.

C. Simulations and Results

The total number of function evaluations for each scenario is 8,200 (18). This corresponds to the evolution of the 200 individuals over the 40 generations and includes the evaluation of the initial population before new individuals can be evolved. Each simulation takes, on average, around 150 minutes on a 64-bit Windows 10 operating system, running on a 2.70 GHz Intel Core i7 with two cores and 16.0 GB of RAM. The three scenarios devised to verify the feasibility of the proposed methodology are set forth below.

Scenario 1: It focuses on the impact of the measurement time delay distribution on the Pareto-optimal fronts. Three cases are considered in which the delay is uniformly distributed: *Case 1.1*: wide range, $\tau_d \sim U[0.05, 0.35]$ s, *Case 1.2*: $\tau_d \sim U[0.10, 0.30]$ s, and *Case 1.3*: narrow range, $\tau_d \sim U[0.15, 0.25]$ s. The rated power of the charging stations, $P_{cluster}$, is set at 10 kW for private stations and 22 kW for public charging stations. The Pareto-optimal fronts for the different cases studied in *Scenario 1* are shown in Fig. 6.

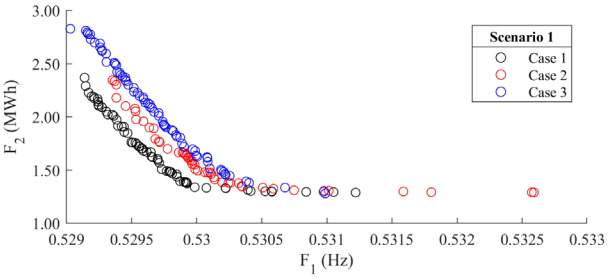

Fig. 6. Pareto-optimal fronts for *Scenario 1* – Impact of the measurement time delay.

Each point represents a combination of the control variables that minimise the objective functions. The horizontal part of the front remains constant for different cases. However, the solutions obtained for *Case 1.1*, when the time delay distribution is wide, dominate the solutions for *Cases 1.2* and *1.3*, when a narrower distribution is explored. Solutions that lie on the flat region, such as those between 0.5305 Hz and 0.5325 Hz, the present poor trade-off between objectives, since a small reduction in the injected energy causes a relatively significant increase to the maximum frequency deviation. More reasonable

solutions seem to be those that lie close to the knee of the curve as they provide a better trade-off between objectives.

Scenario 2: The effect of the public charging stations rated power is explored in this scenario with three cases: *Case 2.1*: $P_{cluster}$ = 10 kW, *Case 2.2*: $P_{cluster}$ = 22 kW, and *Case 2.3*: $P_{cluster}$ = 50 kW. Fast and rapid public charging stations are considered, and the rated power of the private chargers is fixed at 10 kW [30]. For this scenario, the measurement time delay in the EV clusters is modelled with a uniform PDF in which $\tau_d \sim U[0.10, 0.30]$ s. The Pareto-optimal fronts for the cases considered in *Scenario 2* are shown in Fig. 7 (a). The solutions obtained in *Case 2.3* present higher injected energy and consequently, lower frequency deviation than those obtained in *Case 2.1* and *2.2*. This suggests that the effect of increasing the rated power of the charging stations is of reducing the maximum frequency deviation but at the cost of increasing the injected energy from the clusters. More importantly, when the rated power of the charging stations increases, so does the spread of the solutions on the optimal front, which translates into more options for the decision-maker. Useful metrics such as the average Pareto distance and spread are detailed in the Appendix. From Fig. 7 (b) one can observe the evolution of the maximum constraints as the optimisation process progresses. After a maximum in the first generation, the algorithm finds suitable population members, without constraint violations, from around the 30-*th* generation.

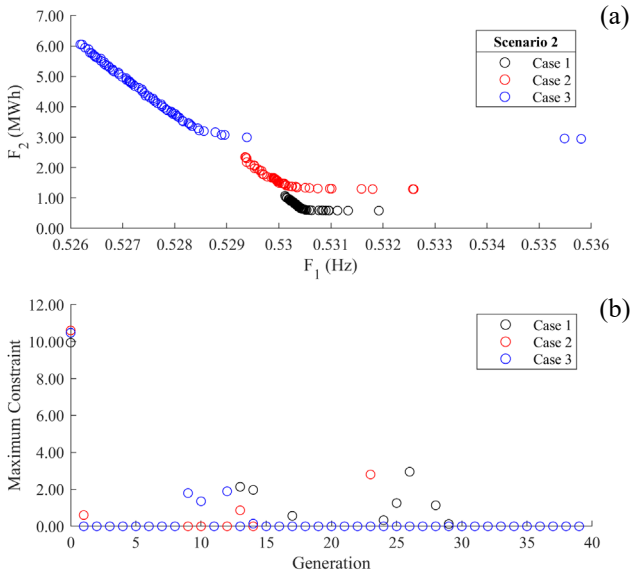

Fig. 7. (a) Pareto-optimal fronts for *Scenario 2* – Impact of the rated power of charging stations. (b) Evolution of the maximum constraint violation during the optimisation.

Scenario 3: It evaluates the sensitivity of the Pareto-front to a ±10% change in the filter time constant T_f. The measurement time delays are set as per *Scenario 2,* and the rated power of the EV charger is fixed as per *Scenario 1*. The values used for the low-pass filter constant are *Case 3.1*: T_f= 0.45 s, *Case 3.2*: T_f= 0.50 s, and *Case 3.3*: T_f= 0.55 s. Fig. 8 (a) shows the optimal Pareto-fronts for the cases studied in *Scenario 3*. It is observed that the solutions obtained in *Case 3.3* dominate those got in *Cases 3.1* and *3.2*. This suggests that for a given value of maximum frequency deviation, in this case, measured by F_1, the amount of energy injected by the EVs connected to public charging stations, showed by F_2, declines when the low-pass filter value T_f is increased. This difference between the fronts is more pronounced for lower values of F_1 that do not require significant V2G energy contribution. For larger values of F_1, the Pareto-fronts converge since the energy required from the EV clusters falls, and the filter impact becomes less relevant.

To observe the impact on the SFR after choosing different sets of control variables from the Pareto-optimal front, two solutions are plotted in Fig. 8 (b). Solution *A* derives from *Case 3.3* and corresponds to a high energy injection from the EV clusters while solution *B* stems from *Case 3.2* and presents a larger frequency deviation and lower energy throughput.

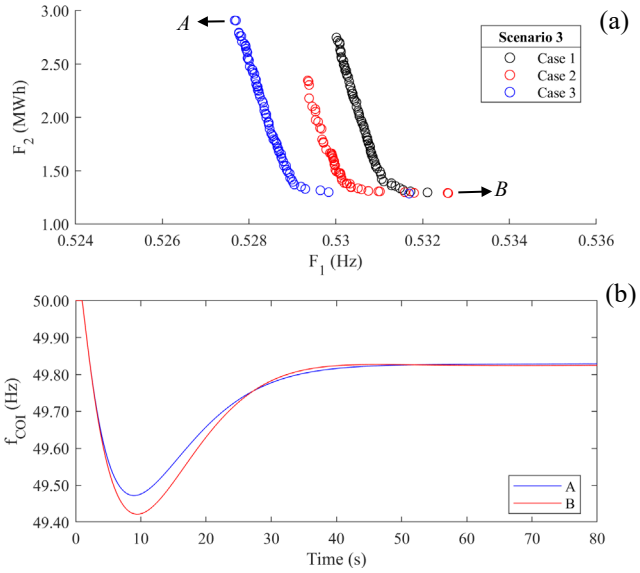

Fig. 8. (a) Pareto-optimal fronts for *Scenario 3* – Sensitivity to filter time constant T_f. (b) Time response of the f_{COI} (10) for different trade-off solutions.

V. Conclusion

The main goal of the current study was to develop a methodology, based on multi-objective techniques, to optimise the provision of FFR from EV clusters following a large power system unbalance. Network security constraints, such as limitations in the inter-area power flows and rate of change of frequency, are included in the proposed methodology. An advantage of the proposed method is that it allows for the objectives and constraints to be handled simultaneously, therefore reducing the simulation time. The insights gained from this study may be of help to decision-makers, such as TSOs and EV aggregating entities involved in the ancillary services market. It is essential to highlight that the decision-maker must select one solution from the Pareto-optimal front presented, based on different techno-economic criteria which fall outside the scope of this paper. The procedure outlined, however, reveals the shape of the Pareto-optimal front to the decision-maker, which makes up a great advantage when choosing the appropriate solution. Further research might explore the impact of more detailed power system models on the Pareto-optimal fronts obtained.

VI. Appendix

Key performance indicators of the proposed methodology.

Scenario. Case	Overall run-time (min)	Function evaluations	Maximum constraint	Average Pareto distance	Average Pareto spread
1.1	138.1	8,201	0	0.0083	0.8985
1.2	293.5	8,201	0	0.0059	0.7274
1.3	134.7	8,201	0	0.0054	0.2567
2.1	179.9	8,201	0	0.0111	0.4829
2.2	222.6	8,201	0	0.0057	0.6744
2.2	156.3	8,201	0	0.0085	0.8928
3.1	147.7	8,201	0	0.0033	0.5948
3.2	147.8	8,201	0	0.0124	0.5408
3.3	349.01	8,201	0	0.0051	0.2729

VII. References

[1] H. R. Chamorro, I. Riaño, R. Gerndt, I. Zelinka, F. Gonzalez-Longatt, and V. K. Sood, "Synthetic inertia control based on fuzzy adaptive differential evolution," *Int. J. Electr. Power Energy Syst.*, vol. 105, no. September 2017, pp. 803–813, Feb. 2019.

[2] F. Sanchez, J. Cayenne, F. Gonzalez-Longatt, and J. L. Rueda, "Controller to Enable the Enhanced Frequency Response Services from a Multi-Electrical Energy Storage System," *IET Gener. Transm. Distrib.*, Nov. 2018.

[3] Zhenpo Wang and Shuo Wang, "Grid Power Peak Shaving and Valley Filling Using Vehicle-to-Grid Systems," *IEEE Trans. Power Deliv.*, vol. 28, no. 3, pp. 1822–1829, Jul. 2013.

[4] F. Mwasilu, J. J. Justo, E.-K. Kim, T. D. Do, and J.-W. Jung, "Electric vehicles and smart grid interaction: A review on vehicle to grid and renewable energy sources integration," *Renew. Sustain. Energy Rev.*, vol. 34, pp. 501–516, Jun. 2014.

[5] I. International Energy Agency, "Global EV Outlook 2018," 2018. [Online]. Available: https://www.iea.org/gevo2018/. [Accessed: 12-Jun-2019].

[6] National Grid, "Future Energy Scenarios," 2017. [Online]. Available: http://fes.nationalgrid.com/fes-document/. [Accessed: 06-Jun-2018].

[7] W. Kempton and J. Tomić, "Vehicle-to-grid power fundamentals: Calculating capacity and net revenue," *J. Power Sources*, vol. 144, no. 1, pp. 268–279, Jun. 2005.

[8] J. Geske and D. Schumann, "Willing to participate in vehicle-to-grid (V2G)? Why not!," *Energy Policy*, vol. 120, no. September 2018, pp. 392–401, Sep. 2018.

[9] Cenex, "Ebbs and Flows of Energy Systems." [Online]. Available: https://www.cenex.co.uk/energy/vehicle-to-grid/efes/. [Accessed: 13-Apr-2019].

[10] EDF_Energy, "EDF Energy and Nuvve Corporation announce plans to install 1,500 smart electric chargers in the United Kingdom." [Online]. Available: https://www.edfenergy.com/media-centre/news-releases/edf-energy-and-nuvve-corporation-announce-plans-install-1500-smart. [Accessed: 13-Apr-2019].

[11] Nissan, "Nissan and Enel launch vehicle-to-grid trial," *Nissan Insider*. [Online]. Available: http://nissaninsider.co.uk/nissan-and-enel-launch-vehicle-to-grid-trial/. [Accessed: 13-Apr-2019].

[12] Energyst, "2019 EV Report Survey." [Online]. Available: https://theenergyst.com/EV/. [Accessed: 13-Apr-2019].

[13] F. Sánchez, F. Gonzalez-Longatt, J. L. Rueda, and P. Palensky, "Impact of Electric Vehicle Charging Control on the Frequency Response : Study of the GB System," in *2018 IEEE PES Innovative Smart Grid Technologies Conference Europe, ISGT-Europe 2018 - Proceedings*, 2018, pp. 3–8.

[14] C. Ziras, J. Hu, S. You, and H. W. Bindner, "Modelling the aggregated dynamic response of electric vehicles," in *2017 IEEE PES Innovative Smart Grid Technologies Conference Europe, ISGT-Europe 2017 - Proceedings*, 2018, vol. 2018-Janua, pp. 1–6.

[15] Thomas Krechel; F. Sanchez; F. Gonzalez-Longatt; H. Chamorro; Jose Luis Rueda, "Transmission System Friendly Micro-grids: An option to provide Ancillary Services," in *Distributed Energy Resources in Microgrids*, R. K. Chauhan; and K. Chauhan, Eds. Elsevier, 2019.

[16] K. Deb and R. Datta, "A fast and accurate solution of constrained optimization problems using a hybrid bi-objective and penalty function approach," *2010 IEEE World Congr. Comput. Intell. WCCI 2010 - 2010 IEEE Congr. Evol. Comput. CEC 2010*, pp. 1–8, 2010.

[17] R. Datta and K. Deb, "An adaptive normalization based constrained handling methodology with hybrid bi-objective and penalty function approach," *2012 IEEE Congr. Evol. Comput. CEC 2012*, pp. 1–8, 2012.

[18] S. S. Guggilam, C. Zhao, E. Dall'Anese, Y. C. Chen, and S. V. Dhople, "Optimizing Power–Frequency Droop Characteristics of Distributed Energy Resources," *IEEE Trans. Power Syst.*, vol. 33, no. 3, pp. 3076–3086, May 2018.

[19] M. Ramírez, R. Castellanos, G. Calderón, and O. Malik, "Placement and sizing of battery energy storage for primary frequency control in an isolated section of the Mexican power system," *Electr. Power Syst. Res.*, vol. 160, pp. 142–150, Jul. 2018.

[20] M. Esmaili and A. Goldoust, "Multi-objective optimal charging of plug-in electric vehicles in unbalanced distribution networks," *Int. J. Electr. Power Energy Syst.*, vol. 73, pp. 644–652, 2015.

[21] S. You, J. Hu, and C. Ziras, "An Overview of Modeling Approaches Applied to Aggregation-Based Fleet Management and Integration of Plug-in Electric Vehicles," *Energies*, vol. 9, no. 11, p. 968, Nov. 2016.

[22] M. Marinelli, S. Martinenas, K. Knezović, and P. B. Andersen, "Validating a centralized approach to primary frequency control with series-produced electric vehicles," *Adv. Life Course Res.*, vol. 7, pp. 63–73, 2016.

[23] V. T. Sæmundsson, M. Rezkalla, A. Zecchino, and M. Marinelli, "Aggregation of Single-phase Electric Vehicles for Frequency Control Provision Based on Unidirectional Charging," *52nd Int. Univ. Power Eng. Conf.*, pp. 1–6, 2017.

[24] D. Doheny and M. Conlon, "Investigation into the local nature of rate of change of frequency in electrical power systems," in *2017 52nd International Universities Power Engineering Conference (UPEC)*, 2017, vol. 2, no. 1, pp. 1–6.

[25] K. Deb, A. Pratap, S. Agarwal, and T. Meyarivan, "A Fast and Elitist Multiobjective Genetic Algorithm: NSGA-II," *IEEE Trans. Evol. Comput.*, vol. 6, no. 2, pp. 182–197, 2002.

[26] A. Nasri, A. Abdollahi, M. Rashidinejad, and M. Hadi Amini, "Probabilistic–possibilistic model for a parking lot in the smart distribution network expansion planning," *IET Gener. Transm. Distrib.*, vol. 12, no. 13, pp. 3363–3374, Jul. 2018.

[27] K. Deb, "An efficient constraint handling method for genetic algorithms," *Comput. Methods Appl. Mech. Eng.*, vol. 186, no. 2–4, pp. 311–338, Jun. 2000.

[28] R. Datta and K. Deb, "An Adaptive Normalization based Constrained Handling," *2012 IEEE Congr. Evol. Comput.*, pp. 1–8, 2012.

[29] L. Saarinen, P. Norrlund, U. Lundin, E. Agneholm, and A. Westberg, "Full-scale test and modelling of the frequency control dynamics of the Nordic power system," *IEEE Power Energy Soc. Gen. Meet.*, vol. 2016-Novem, 2016.

[30] International Energy Agency, "Nordic EV Outlook 2018," 2018. [Online]. Available: https://www.nordicenergy.org/publications/nordic-ev-outlook-2018/. [Accessed: 03-Jul-2019].

[31] J. Kester, L. Noel, G. Zarazua de Rubens, and B. K. Sovacool, "Promoting Vehicle to Grid (V2G) in the Nordic region: Expert advice on policy mechanisms for accelerated diffusion," *Energy Policy*, vol. 116, no. February, pp. 422–432, May 2018.

[32] A. Zecchino, A. M. Prostejovsky, C. Ziras, and M. Marinelli, "Large-scale provision of frequency control via V2G: The Bornholm power system case," *Electr. Power Syst. Res.*, vol. 170, no. December 2018, pp. 25–34, May 2019.

[33] M. Rezkalla, A. Zecchino, S. Martinenas, A. M. Prostejovsky, and M. Marinelli, "Comparison between synthetic inertia and fast frequency containment control based on single phase EVs in a microgrid," *Appl. Energy*, vol. 210, pp. 764–775, Jan. 2018.

[34] Y. Mu, J. Wu, J. Ekanayake, N. Jenkins, and H. Jia, "Primary Frequency Response From Electric Vehicles in the Great Britain Power System," *Smart Grid, IEEE Trans.*, vol. 4, no. 2, pp. 1142–1150, Jun. 2013.

[35] G. Li, T. Goel, and N. Stander, "Assessing the Convergence Properties of NSGA-II for Direct Crashworthiness Optimization," *Design*, no. 1, pp. 31–38.

[36] C. Versèle, O. Deblecker, Z. De Grève, and J. Lobry, "Multiobjective optimal design of a voltage supply inverter fed in-wheel synchronous motor," *2010 IEEE Veh. Power Propuls. Conf. VPPC 2010*, 2010.